Spin-Peierls Instability of Three-Dimensional Spin Liquids with Majorana Fermi Surfaces

Maria Hermanns, Simon Trebst, and Achim Rosch

Institute for Theoretical Physics, University of Cologne, 50937 Cologne, Germany

Three-dimensional (3D) variants of the Kitaev model can harbor gapless spin liquids with a Majorana Fermi surface on certain tricoordinated lattice structures such as the recently introduced hyperoctagon lattice. Here, we investigate Fermi surface instabilities arising from additional spin exchange terms (such as a Heisenberg coupling) which introduce interactions between the emergent Majorana fermion degrees of freedom. We show that independent of the sign and structure of the interactions, the Majorana surface is always unstable. Generically, the system spontaneously doubles its unit cell at exponentially small temperatures and forms a spin liquid with line nodes. Depending on the microscopics, further symmetries of the system can be broken at this transition. These spin-Peierls instabilities of a 3D spin liquid are closely related to BCS instabilities of fermions.

The interplay of frustration and correlations in quantum magnets engenders a rich variety of quantum states with fractional excitations that are collectively referred to as quantum spin liquids (QSLs) [1]. Archetypal instances of such states include gapped topological QSLs with anyonic quasiparticle excitations, as well as gapless QSLs where emergent spinon excitations form nodal structures such as Dirac points, Fermi lines, and Fermi surfaces reminiscent of metallic states. A family of such gapless QSLs is realized in two- and three-dimensional variants of the Kitaev model [2] in which a high level of exchange frustration is induced by competing bond-directional interactions of the form

$$H_{\text{Kitaev}} = J \sum_{\gamma \text{links}} S_i^\gamma S_j^\gamma. \qquad (1)$$

Here spin-1/2 moments S on sites i and j are coupled via an Ising-like exchange whose easy axis aligns with the $\gamma = x, y, z$ orientation of the bonds of the underlying tricoordinated lattices. Kitaev's seminal solution [2] of this model for the honeycomb lattice allows us to analytically track the fractionalization of the original spin-1/2 moments into emergent massless Majorana fermions (spinons) and massive $\mathbb{Z}_2$ gauge excitations (visons). The collective QSL ground state is a (semi-)metallic state formed by the itinerant Majorana fermions. The qualitative nature of this Majorana metal turns out to depend on the underlying lattice: for the two-dimensional honeycomb lattice, the itinerant Majorana fermions form two Dirac cones [2] (akin to the well-known electronic band structure of graphene), while for the three-dimensional hyperhoneycomb and hyperoctagon lattices, the gapless Majorana modes form a Fermi line [3] and an entire Fermi surface [4], respectively. In the presence of additional time-reversal symmetry breaking terms, the Majorana fermions (on the hyperhoneycomb lattice) can even form a topological semimetal

with Weyl nodes [5]. Interest in such three-dimensional Kitaev models has been sparked by the recent experimental observation of spin-orbit entangled $j = 1/2$ Mott insulators with strong bond-directional interactions of the form (1) in the iridates $(\beta, \gamma) - \text{Li}_2\text{IrO}_3$ [6–9], where the iridium sites form three-dimensional, tricoordinated lattice structures. The synthesis of such three-dimensional Kitaev structures expands an intense ongoing search for solid-state realizations of the original two-dimensional Kitaev model, which—following the early theoretical guidance of Khaliullin and co-workers [10]—has put materials such as the layered iridates Na_2IrO_3, $\alpha - \text{Li}_2\text{IrO}_3$ [11] and, more recently, $\alpha - \text{RuCl}_3$ [12] into focus.

In this Letter, we concentrate on three-dimensional Kitaev spin liquids characterized by Majorana Fermi surfaces and show that they generically dimerize, i.e., double their unit cell at low temperature. This instability can be viewed as a generalization of the spin-Peierls transition in one-dimensional systems [13,14] or, more generally, of the tendency of frustrated low-dimensional spin systems to form valence-bond solids [15]. The spin-Peierls instability of (quasi-)one-dimensional spin systems describes that an arbitrarily small coupling of a spin chain to classical lattice degrees of freedom leads at low temperature to a dimerization and a gap in the spin system [13,14]: the energy gain by opening the gap is larger than the energy needed to distort the lattice. When the phonon mode is, however, treated quantum mechanically, a dimerization occurs only when a critical coupling strength is reached [16]. As we show, for the 3D Kitaev spin liquid, a variant of the spin-Peierls transition occurs at low T even in the *absence* of lattice degrees of freedom and for arbitrarily weak perturbations. Notably, the result of this instability is not a short-range valence-bond ordered state, but still a QSL—yet one, in which the original Majorana Fermi surface has collapsed into a line of gapless modes.

Model system.—For concreteness, we focus our analysis on a specific 3D Kitaev model and return to a more general discussion later. We look at the Kitaev model defined on the so-called hyperoctagon lattice depicted in Fig. 1. For this system a gapless QSL ground state with a Majorana Fermi surface was established in Ref. [4], to which we also refer the reader for technical details of the analytical solution of this model. In brief, the spin degrees of freedom fractionalize to itinerant Majorana fermions interacting with static $\mathbb{Z}_2$ gauge fields [2]. In the (flux-free) ground state sector of the $\mathbb{Z}_2$ gauge field, the original spin model (1) reduces to a free hopping model of Majorana fermions

$$
\begin{aligned}
H_0 = -iJ \sum_{\mathbf{R}} & c_1(\mathbf{R})c_3(\mathbf{R}-\mathbf{a}_2) + c_2(\mathbf{R})c_4(\mathbf{R}-\mathbf{a}_3) \\
& + c_1(\mathbf{R})c_2(\mathbf{R}) - c_3(\mathbf{R})c_4(\mathbf{R}) - c_2(\mathbf{R})c_3(\mathbf{R}) \\
& + c_1(\mathbf{R})c_4(\mathbf{R}-\mathbf{a}_1).
\end{aligned}
\tag{2}
$$

Here, $\mathbf{R}$ is the position of the unit cells within the bcc Bravais lattice (see Fig. 1), each containing four sites labeled by $i = 1, 2, 3, 4$; $\mathbf{a}_j$ are the lattice vectors defined in Fig. 1 and the Majorana operators obey the usual algebra $\{c_i(\mathbf{R}), c_j(\mathbf{R}')\} = 2\delta_{ij}\delta_{\mathbf{R},\mathbf{R}'}$.

Diagonalizing the Hamiltonian (2), one finds that two of the four bands have a gap of order J; the other two bands become gapless on two two-dimensional surfaces in momentum space defined by the equation $\cos k_x + \cos k_y + \cos k_z = -(3/2)$ [4]. The two closed Majorana surfaces are centered around the momenta $\pm\mathbf{k}_0/2$, with $\mathbf{k}_0 = 2\pi(1, 1, 1)$, as illustrated in Fig. 2(a). Note that only $2\mathbf{k}_0$ is a unit vector of the reciprocal lattice, not $\mathbf{k}_0$ itself. Most importantly, there is a perfect nesting condition between the two Majorana surfaces,

$$
\epsilon_{\mathbf{k}} = \epsilon_{\mathbf{k}+\mathbf{k}_0},
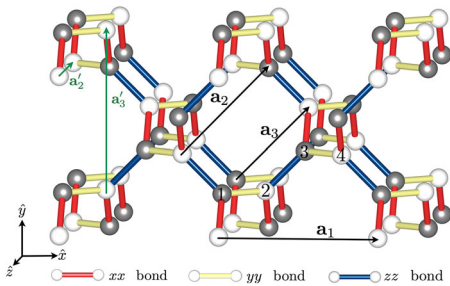\tag{3}
$$

FIG. 1 (color online). The hyperoctagon lattice is a tricoordinated bcc lattice without inversion symmetry (space group $I4_132$) and a four-site unit cell (with atom positions 1, ..., 4 and unit-cell vectors $\mathbf{a}_1$, $\mathbf{a}_2$, and $\mathbf{a}_3$ indicated in the figure). For the definition of the Kitaev model on this lattice, we define nearest-neighbor spin interactions of the S^xS^x, S^yS^y, and S^zS^z type assigned to the green, red, and blue bonds, respectively. The vectors $\mathbf{a}_1$, $\mathbf{a}_2' = \mathbf{a}_2 - \mathbf{a}_3$, and $\mathbf{a}_3' = -\mathbf{a}_1 + \mathbf{a}_2 + \mathbf{a}_3$ are the lattice translation vectors of each of the two sublattices (denoted by white and grey lattice sites).

which is *not* specific to the microscopic Hamiltonian (1) but arises from the peculiar form of *time-reversal symmetry* $\mathcal{T}$ of the underlying spin model realized by [2,4]

$$
c_j(\mathbf{R}) \xrightarrow{\mathcal{T}} (-1)^j e^{i\mathbf{k}_0 \cdot \mathbf{R}} c_j(\mathbf{R}).
\tag{4}
$$

For the following discussion it is convenient to combine the two low-energy Majorana bands into a single band of a (complex) fermion, which allows us to use the more familiar language of superconductors to describe the system. To do so, we denote the low-energy Majorana excitations with momentum $\mathbf{k}$ by $\gamma_{\mathbf{k}}^{1/2}$ with $\epsilon_{\mathbf{k}}^1 \le \epsilon_{\mathbf{k}}^2$. Note that the particle-hole symmetry of Majorana fermions readily implies $\gamma_{\mathbf{k}}^1 = (\gamma_{-\mathbf{k}}^2)^\dagger$, which requires us to either restrict the discussion to half the Brillouin zone or, alternatively, to the upper energy band. Doing the latter, we introduce the Fermion operator $f_{\mathbf{k}}$ by $f_{\mathbf{k}} = (1/\sqrt{2})\gamma_{\mathbf{k}}^2$. This reformulation combines the two Majorana surfaces in Fig. 2(a) into a single Fermi surface of a complex fermion centered around $\mathbf{k}_0/2$; see Fig. 2(b). In terms of the complex fermion, time-reversal symmetry (4) becomes

$$
f_{\mathbf{k}_0/2+\mathbf{k}}^\dagger \xrightarrow{\mathcal{T}} f_{\mathbf{k}_0/2-\mathbf{k}}^\dagger,
\tag{5}
$$

constraining the fermionic energy spectrum to be symmetric relative to $\mathbf{k}_0/2$:

$$
E_{\mathbf{k}_0/2+\mathbf{k}} = E_{\mathbf{k}_0/2-\mathbf{k}}.
\tag{6}
$$

This energy relation naturally leads us to consider pairing terms of the form $f_{\mathbf{k}_0/2+\mathbf{k}}^\dagger f_{\mathbf{k}_0/2-\mathbf{k}}^\dagger$. However, such pairs carry a *finite* momentum $\mathbf{k}_0$ [17] and can therefore only arise in a phase in which translational symmetry is spontaneously broken. Here, we show that such a spontaneous symmetry breaking occurs in the presence of additional spin exchange terms.

Interactions.—Any deviation from the ideal Kitaev model, e.g., by introducing spin-spin interactions of the Heisenberg form, Dzyaloshinskii Moriya interactions, three-spin interactions, etc., will induce interactions of the Majorana fermions. As long as the size of these perturbations is sufficiently small (compared to the
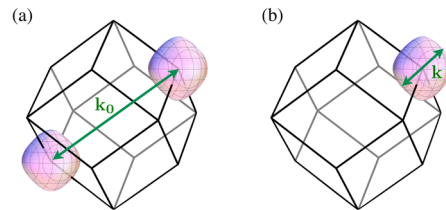

FIG. 2 (color online). (a) Sketch of the two Majorana Fermi surfaces in the Brillouin zone. In the Majorana language, the Peierls instability is due to perfect nesting between the two surfaces. (b) The two Majorana surfaces combine to a single Fermi surface of a (complex) fermion. In the fermionic language, the Peierls instability is the usual BCS instability.

Kitaev interaction J, which, in particular, sets the energy scale for the flux gap), the interaction can be written in terms of the Majorana fermions only (without any contributions from the fluxes) and will remain short ranged. For the hyperoctagon lattice, two types of Majorana interactions turn out to be the most local ones, which are therefore also expected to be the most important ones in an expansion around the Kitaev model [18]. We parametrize them by their overall strength U and an angle α as

$$H_{\text{int}} = -U\Bigg(\cos\alpha\sum_{\mathbf{R}} c_1(\mathbf{R})c_2(\mathbf{R})c_3(\mathbf{R})c_1(\mathbf{R}+\mathbf{a}_2)$$

$$+ \sin\alpha\sum_{\mathbf{R}} c_1(\mathbf{R})c_2(\mathbf{R})c_3(\mathbf{R})c_4(\mathbf{R}) + \text{sym}\Bigg). \quad (7)$$

Note that each term in the above expression is only a single representative of 24 distinct terms obtained by the 48 symmetry transformations of the $I4_132$ symmetry group of the hyperoctagon lattice [19]. When adding, e.g., a nearest-neighbor Heisenberg coupling J_H to the Kitaev model, one expects $U \sim J_H^4/J^3$ [2]. In general, the sizes of U and α will depend on all types of microscopic details and are difficult to predict quantitatively. We therefore analyze the effect of the interactions (7) for varying values of α (and fixed, small U).

To analyze $H_0 + H_{\text{int}}$ for small U, we first project the interaction (7) onto the low-energy degrees of freedom described by the complex f fermions introduced above and obtain

$$H_{\text{eff}} = \sum_{\mathbf{k}}\epsilon_{\mathbf{k}} f_{\mathbf{k}}^\dagger f_{\mathbf{k}} + \sum_{\mathbf{k}_1,\mathbf{k}_2,\mathbf{k}_3} V^1_{\mathbf{k}_1,\mathbf{k}_2,\mathbf{k}_3} f_{\mathbf{k}_1}^\dagger f_{\mathbf{k}_2}^\dagger f_{\mathbf{k}_3} f_{\mathbf{k}_1+\mathbf{k}_2-\mathbf{k}_3}$$

$$+ \sum_{\mathbf{k}_1,\mathbf{k}_2,\mathbf{k}_3} V^2_{\mathbf{k}_1,\mathbf{k}_2,\mathbf{k}_3} f_{\mathbf{k}_1}^\dagger f_{\mathbf{k}_2}^\dagger f_{\mathbf{k}_3}^\dagger f_{-\mathbf{k}_1-\mathbf{k}_2-\mathbf{k}_3}^\dagger + \text{H.c.} \quad (8)$$

The momentum dependence of $V^{1,2}$ can easily be obtained numerically using Eq. (7), the eigenmodes of H_0, and the definition $f_{\mathbf{k}}^\dagger$ given above. Note that symmetry-allowed terms of the form $f_{\mathbf{k}}^\dagger f_{-\mathbf{k}}^\dagger$ or $f_{\mathbf{k}_1}^\dagger f_{\mathbf{k}_2}^\dagger f_{\mathbf{k}_3}^\dagger f_{\mathbf{k}_1+\mathbf{k}_2+\mathbf{k}_3}$ do not contribute to the low-energy sector, as at least one of the momenta is far away from the Fermi surface.

Pairing instability.—As H_0 can be written as noninteracting spinless fermions, it is not surprising that the pairing instability due to terms such as $f_{\mathbf{k}_0/2+\mathbf{k}}^\dagger f_{\mathbf{k}_0/2-\mathbf{k}}^\dagger$ is governed by the same type of logarithms which are responsible for p-wave superconductivity [22]. For small U, one can therefore expect that dimerization sets in below a transition temperature

$$T_c = E_{0,\alpha}e^{-c_\alpha J/U} \quad \text{for } U \ll J, \quad (9)$$

where $E_{0,\alpha}$ is an energy scale of order J. The dimensionless constant c_α can be computed exactly from a one-loop renormalization group calculation or, alternatively, from a

BCS mean-field calculation. In the following we use BCS theory to compute T_c and the structure of the order parameter. Our approach allows us to calculate c_α exactly, but, unfortunately, not the prefactor $E_{0,\alpha}$ [23]. Because of the absence of further nesting effects, only the pairing channel is divergent for $U \to 0$, and therefore this is the only instability for sufficiently weak perturbations around the Kitaev point.

To describe the dimerized phase, we consider the BCS-style Hamiltonian

$$H_{\text{BCS}} = \sum_k \epsilon_k f_{\mathbf{k}}^\dagger f_{\mathbf{k}} + \sum_{k_x>0}\Delta_{\mathbf{k}} f_{\mathbf{k}_0/2+\mathbf{k}}^\dagger f_{\mathbf{k}_0/2-\mathbf{k}}^\dagger + \text{H.c.}, \quad (10)$$

where the odd order parameter, $\Delta_{\mathbf{k}} = -\Delta_{-\mathbf{k}}$, is computed from the mean-field equation

$$\Delta_{\mathbf{k}} = 2\sum_{\mathbf{q}} V^1_{\mathbf{k}_0/2+\mathbf{k},\mathbf{k}_0/2-\mathbf{k},\mathbf{k}_0/2+\mathbf{q}}\langle f_{\mathbf{k}_0/2+\mathbf{q}} f_{\mathbf{k}_0/2-\mathbf{q}}\rangle$$

$$+ 12 V^2_{\mathbf{k}_0/2+\mathbf{k},\mathbf{k}_0/2-\mathbf{k},\mathbf{k}_0/2+\mathbf{q}}\langle f_{\mathbf{k}_0/2+\mathbf{q}}^\dagger f_{\mathbf{k}_0/2-\mathbf{q}}^\dagger\rangle, \quad (11)$$

where we assumed that the interactions in Eq. (8) have been completely antisymmetrized with respect to the fermionic operators. All expectation values are computed with H_{BCS}. Note that, in contrast to the standard BCS theory, there is no $U(1)$ symmetry. It turns out that time-reversal symmetry (5) is *not* spontaneously broken, which leads to a purely imaginary $\Delta_{\mathbf{k}}$, $\Delta_{\mathbf{k}}^* = -\Delta_{\mathbf{k}}$. The latter, together with $\Delta_{\mathbf{k}} = -\Delta_{-\mathbf{k}}$, already implies that pairing cannot gap the Fermi surface completely, but only reduce it to an odd number of lines.

To simplify Eq. (11) and to solve it with high numerical precision to leading logarithmic order, we rewrite the $\mathbf{q}$ integration into an integral on the Fermi surface and an energy integration perpendicular to it, $\int d^3\mathbf{q} = \int_{\text{FS}} d^2\mathbf{k}_F \int N_{\mathbf{k}_F}(\epsilon)d\epsilon$. We furthermore approximate the directional dependent density of state by its value of the Fermi surface, $N_{\mathbf{k}_F}(0) = [1/(2\pi)^3 v_F(\mathbf{k}_F)]$ for $-2J < \epsilon < 2J$. Similarly, we approximate both $\Delta_{\mathbf{k}}$ and the matrix elements of V^1 and V^2 by their values on the Fermi surface. This allows for an accurate evaluation of the ϵ integration, $\int d\epsilon \langle f_{\mathbf{k}_0/2+\mathbf{q}} f_{\mathbf{k}_0/2-\mathbf{q}}\rangle \approx \Delta_{\mathbf{q}_F}\int_0^{2J} d\epsilon\{[\tanh\sqrt{\epsilon^2+|\Delta_{\mathbf{q}_F}|^2}/(2T)]/[\sqrt{\epsilon^2+|\Delta_{\mathbf{q}_F}|^2}]\}$. The last term is evaluated numerically, but it is also well described by $\Delta_{\mathbf{q}_F}\ln[4J/\sqrt{|\Delta_{\mathbf{q}_F}|^2 + (1.762T)^2}]$. For the plots of this Letter, we discretize the Fermi surface using a total of 1344 patches.

Phase diagram.—Using the largest eigenvalue of the linearized BCS equation (11), one can directly determine c_α in Eq. (9) with $E_{0,\alpha} \approx 2.27J$ within our cutoff scheme (for a plot of c_α, see the Supplemental Material [20]). For $0 < \alpha < 4.65$ the eigenvalue is threefold degenerate. The three eigenvectors form an irreducible representation of the point group O and transform like k_x, k_y, and k_z (the T_1
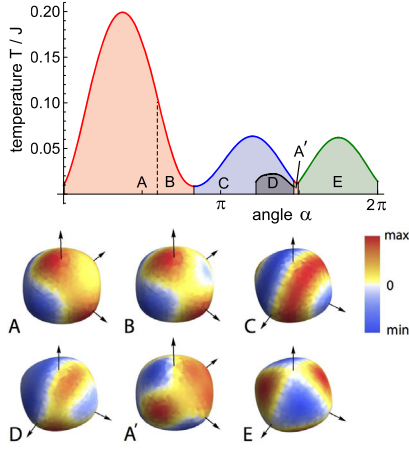
FIG. 3 (color online). (Upper panel) Phase diagram for $U = 0.4J$ as a function of the angle α. There are four different phases distinguished by symmetry (see Table I). (Lower panel) For the five phases $A - E$, the angular distribution of the order parameter Δ_q on the Majorana surface is shown ($\alpha = 0.5\pi, 0.7\pi, \pi, 1.35\pi, 1.48\pi, 1.75\pi$). The coordinate systems have been rotated around the z axis for better visibility.

TABLE I. Overview of the symmetry-broken phases; see Fig. 3. In all phases the unit cell is doubled. The first column shows schematically the symmetry of the order parameter (momenta measured from $k_0/2$). Furthermore, the point group of the symmetry-broken phase, the number of domains, and the number of line nodes are tabulated.

	Order parameter	Point group	Domains	Line nodes
A, A'	$k_x + k_y + k_z$	D_3 (32)	8	1
B	$k_x + k_y + k_z$	D_3 (32)	8	3
C	k_x	D_4 (422)	6	3
D	$c_1 k_x + c_2 k_y$	C_2 (2)	24	3
E	$k_x k_y k_z$	O (432)	2	3 (crossing)

representation; see the Supplemental Material [20]). For $4.65 < \alpha < 2\pi$, in contrast, the eigenvalue is unique and the eigenvector transforms like $k_x k_y k_z$ (the A_2 representation). Analyzing the BCS equation beyond the linear approximation, one obtains the phase diagram shown for $U = 0.4J$ in the middle panel of Fig. 3 as a function of temperature T and α. For other values of U one obtains very similar phase diagrams, but all transition temperatures and the ratio of the largest and smallest T_c change exponentially according to Eq. (9).

We find five different phases, denoted $A - E$ in Fig. 3, which are distinguished by symmetry and/or the number of line nodes; the corresponding distribution of order parameters is shown in the lower panel of Fig. 3. In Table I an overview of the properties of the symmetry-broken phases is given. In all phases the unit cell has doubled. In phase E this is the only broken symmetry. In phases $A - D$ other lattice symmetries are broken besides the translational symmetry. As at T_c the eigenvalue c_α is threefold degenerate, the phase diagram can be understood best in terms of a three-component order parameter, $\Phi = (\Phi_1, \Phi_2, \Phi_3)$, where Φ_i corresponds to an eigenvector transforming like k_i. Close to T_c, one can use a Landau description of the free energy of the form

$$F \approx (T - T_c)\Phi^2 + g(\Phi^2)^2 + g'(\Phi_1^4 + \Phi_2^4 + \Phi_3^4) + O(\Phi^6). \quad (12)$$

It predicts that just below T_c the order parameter points for $g' > 0$ in one of the (111) directions (phases A, A', and B, colored in red in Fig. 3). The order parameter therefore has a 120°-rotation symmetry around this axis; see also the lower panel in Fig. 3. In the crystal structure this (111)

direction will be shortened or elongated (depending on the sign of the coupling to the lattice), allowing for eight possible domains in total. For $g' < 0$, in contrast, the order parameter points along a (100) direction (phase C with six domains) and the lattice will shrink or expand along that direction. Interestingly, it turns out that all phases besides the phase A are characterized by three line nodes instead of a single one; see Fig. 3. The simple Landau theory (12) can fail at low T and, indeed, phase D cannot be described by terms up to order Φ^4. Here, further symmetries are broken (see Table I), Φ points in a low-symmetry direction, e.g., $(c_1, c_2, 0)$, and the ordered phase is characterized by 24 different domains. In this case the only remaining symmetry of the order parameter is that it changes sign by a 180° rotation around the (001) axis.

Experimental signatures.—The spin-Peierls instability gives rise to a distinct experimental fingerprint, which could facilitate the ongoing search for Kitaev spin liquids. In thermodynamics, one expects to observe (i) the absence of magnetic order breaking time-reversal symmetry, (ii) an approximately constant specific heat coefficient c_v/T over a wide intermediate temperature range (indicative of the Majorana Fermi surface), (iii) a structural phase transition with unit-cell doubling at small temperatures T_c, and (iv) a low-temperature specific heat with $c_v/T \approx T$ (indicative of the nodal lines) with possible logarithmic corrections (arising from the crossing points of the nodal lines for phase E). Besides the structural phase transition discussed here, three-dimensional $\mathbb{Z}_2$ gauge theories also show a finite-T phase transition [24–26] of (inverted) Ising universality class. Note that we have implicitly assumed in our calculation that the T_c of the structural transition is well below this transition temperature where flux lines proliferate.

The doubling of the unit cell will generically be reflected both in valence-bond correlations and also shifts of the position of atoms [20]. Consider, for example, spins located on one of the threefold rotation axes, $\mathbf{r}_0 + n\mathbf{v}$, of the system with, e.g., $\mathbf{v} = (1/2, 1/2, 1/2)$. They obtain a staggered expectation value proportional to the order parameter Δ,

$$\langle \mathbf{S}(\mathbf{r}_0 + n\mathbf{v})\mathbf{S}(\mathbf{r}_0 + (n+1)\mathbf{v})\rangle \sim (-1)^n \Delta. \quad (13)$$

Summary.—We have shown that a time-reversal symmetric spin liquid with a Majorana surface is always unstable and spontaneously undergoes a spin-Peierls transition to a nodal QSL at low temperatures. We expect that this is a generic property of Majorana surfaces. To show this, it is useful to classify time-reversal invariant Majorana systems by the value of the vector $\mathbf{k}_0$ characterizing the time-reversal operation in Eq. (4) or, equivalently, Eq. (5). If k_0 vanishes, terms of the form $f^\dagger_{\mathbf{k}_0/2+\mathbf{k}} f^\dagger_{\mathbf{k}_0/2-\mathbf{k}}$ occur even in the absence of symmetry breaking and—instead of a Fermi surface—only a state with nodal line forms [3,26]. Fermi surfaces therefore exist only for a finite $\mathbf{k}_0$. In this case, however, time-reversal invariance guarantees the existence of a BCS-type instability. As any interaction of Majorana excitations always involves four different sites, the momentum-dependent interaction will always have an attractive channel leading to a transition where Majorana pairs condensate at finite momentum $\mathbf{k}_0$. We therefore expect that Majorana surfaces can only survive for $T \to 0$ in cases where time-reversal symmetry is broken either spontaneously or explicitly, e.g., by an external magnetic field—a scenario which we plan to investigate in the future.

[1] For a recent review, see, e. g., L. Balents, Spin liquids in frustrated magnets, Nature (London) **464**, 199 (2010).

[2] A. Kitaev, Anyons in an exactly solved model and beyond, Ann. Phys. (Amsterdam) **321**, 2 (2006).

[3] S. Mandal and N. Surendran, Exactly solvable Kitaev model in three dimensions, Phys. Rev. B **79**, 024426 (2009).

[4] M. Hermanns and S. Trebst, Quantum spin liquid with a Majorana Fermi surface on the three-dimensional hyperoctagon lattice, Phys. Rev. B **89**, 235102 (2014).

[5] M. Hermanns, K. O'Brien, and S. Trebst, Weyl Spin Liquids, Phys. Rev. Lett. **114**, 157202 (2015).

[6] T. Takayama, A. Kato, R. Dinnebier, J. Nuss, and H. Takagi, Hyperhoneycomb Iridate β-Li$_2$IrO$_3$ as a Platform for Kitaev Magnetism, Phys. Rev. Lett. **114**, 077202 (2015).

[7] K. A. Modic, T. E. Smidt, I. Kimchi, N. P. Breznay, A. Biffin, S. Choi, R. D. Johnson, R. Coldea, P. Watkins-Curry, G. T. McCandless, J. Y. Chan, F. Gandara, Z. Islam, A. Vishwanath, A. Shekhter, R. D. McDonald, and J. G. Analytis, Realization of a three-dimensional spin-anisotropic harmonic honeycomb iridate, Nat. Commun. **5**, 4203 (2014).

[8] A. Biffin, R. D. Johnson, S. Choi, F. Freund, S. Manni, A. Bombardi, P. Manuel, P. Gegenwart, and R. Coldea, Unconventional magnetic order on the hyperhoneycomb Kitaev lattice in β-Li$_2$IrO$_3$: Full solution via magnetic resonant x-ray diffraction, Phys. Rev. B **90**, 205116 (2014).

[9] A. Biffin, R. D. Johnson, I. Kimchi, R. Morris, A. Bombardi, J. G. Analytis, A. Vishwanath, and R. Coldea, Noncoplanar and Counterrotating Incommensurate Magnetic Order Stabilized by Kitaev Interactions in γ-Li$_2$IrO$_3$, Phys. Rev. Lett. **113**, 197201 (2014).

[10] G. Khaliullin, Orbital order and fluctuations in Mott insulators, Prog. Theor. Phys. Suppl. **160**, 155 (2005); G. Jackeli and G. Khaliullin, Mott Insulators in the Strong Spin-Orbit Coupling Limit: From Heisenberg to a Quantum Compass and Kitaev Models, Phys. Rev. Lett. **102**, 017205 (2009); J. Chaloupka, G. Jackeli, and G. Khaliullin, Kitaev-Heisenberg Model on a Honeycomb Lattice: Possible Exotic Phases in Iridium Oxides A$_2$IrO$_3$, Phys. Rev. Lett. **105**, 027204 (2010).

[11] Y. Singh, S. Manni, J. Reuther, T. Berlijn, R. Thomale, W. Ku, S. Trebst, and P. Gegenwart, Relevance of the Heisenberg-Kitaev Model for the Honeycomb Lattice Iridates A$_2$IrO$_3$, Phys. Rev. Lett. **108**, 127203 (2012); S. K. Choi *et al.*, Spin Waves and Revised Crystal Structure of Honeycomb Iridate Na$_2$IrO$_3$, Phys. Rev. Lett. **108**, 127204 (2012); R. Comin *et al.*, Na$_2$IrO$_3$ as a Novel Relativistic Mott Insulator with a 340-meV Gap, Phys. Rev. Lett. **109**, 266406 (2012); F. Ye, S. Chi, H. Cao, B. C. Chakoumakos, J. A. Fernandez-Baca, R. Custelcean, T. F. Qi, O. B. Korneta, and G. Cao, Direct evidence of a zigzag spin-chain structure in the honeycomb lattice: A neutron and x-ray diffraction investigation of single-crystal Na$_2$IrO$_3$, Phys. Rev. B **85**, 180403 (2012); H. Gretarsson *et al.*, Crystal-Field Splitting and Correlation Effect on the Electronic Structure of A$_2$IrO$_3$, Phys. Rev. Lett. **110**, 076402 (2013); H. Gretarsson *et al.*, Magnetic excitation spectrum of Na$_2$IrO$_3$ probed with resonant inelastic x-ray scattering, Phys. Rev. B **87**, 220407 (2013); S. H. Chun, J.-W. Kim, J. Kim, H. Zheng, C. C. Stoumpos, C. D. Malliakas, J. F. Mitchell, K. Mehlawat, Y. Singh, Y. Choi, T. Gog, A. Al-Zein, M. Moretti Sala, M. Krisch, J. Chaloupka, G. Jackeli, G. Khaliullin, and B. J. Kim, Direct evidence for dominant bond-directional interactions in a honeycomb lattice iridate Na$_2$IrO$_3$, Nat. Phys. **11**, 462 (2015).

[12] K. W. Plumb, J. P. Clancy, L. J. Sandilands, V. Vijay Shankar, Y. F. Hu, K. S. Burch, H.-Y. Kee, and Y.-J. Kim, α-RuCl$_3$: A spin-orbit assisted Mott insulator on a honeycomb lattice, Phys. Rev. B **90**, 041112(R) (2014); L. J. Sandilands, Y. Tian, K. W. Plumb, Y.-J. Kim, and K. S. Burch, Scattering Continuum and Possible Fractionalized Excitations in α-RuCl$_3$, Phys. Rev. Lett. **114**, 147201 (2015); H.-S. Kim, V. Vijay Shankar, A. Catuneanu, and H.-Y. Kee, Kitaev magnetism in honeycomb RuCl$_3$ with intermediate spin-orbit coupling, Phys. Rev. B **91**, 241110 (2015); M. Majumder, M. Schmidt, H. Rosner, A. A. Tsirlin, H. Yasuoka, and M. Baenitz, Anisotropic Ru^{3+} 4d^5 magnetism in the α-RuCl$_3$ honeycomb system: Susceptibility, specific heat, and zero-field NMR, Phys. Rev. B **91**, 180401(R) (2015); L. J. Sandilands, Y. Tian, A. A. Reijnders, H.-S. Kim, K. W. Plumb, H.-Y. Kee, Y.-J. Kim, and K. S. Burch, Orbital excitations in the 4d spin-orbit coupled Mott insulator α-RuCl$_3$, arXiv:1503.07593; Y. Kubota, H. Tanaka, T. Ono, Y. Narumi, and K. Kindo, Successive magnetic phase transitions in α-RuCl$_3$: XY-like frustrated magnet on the honeycomb lattice, Phys. Rev. B **91**, 094422 (2015); A. Banerjee, C. A. Bridges, J.-Q. Yan, A. A. Aczel, L. Li, M. B. Stone, G. E. Granroth, M. D. Lumsden, Y. Yiu, J. Knolle, D. L. Kovrizhin, S. Bhattacharjee, R. Moessner, D. A. Tennant, D. G. Mandrus, and S. E. Nagler, Proximate Kitaev quantum spin liquid behaviour in α-RuCl$_3$, arXiv:1504.08037.

[13] E. Pytte, Peierls instability in Heisenberg chains, Phys. Rev. B **10**, 4637 (1974).

[14] M. C. Cross and D. S. Fisher, A new theory of the spin-Peierls transition with special relevance to the experiments on TTFCuBDT, Phys. Rev. B **19**, 402 (1979).

[15] N. Read and S. Sachdev, Spin-Peierls, valence-bond solid, and Néel ground states of low-dimensional quantum anti-ferromagnets, Phys. Rev. B **42**, 4568 (1990).

[16] G. S. Uhrig, Nonadiabatic approach to spin-Peierls transitions via flow equations, Phys. Rev. B **57**, R14004 (1998); A. W. Sandvik and D. K. Campbell, Spin-Peierls Transition in the Heisenberg Chain with Finite-Frequency Phonons, Phys. Rev. Lett. **83**, 195 (1999).

[17] Note that for other three-dimensional, tricoordinated lattices (such as the hyperhoneycomb lattice), $\mathbf{k}_0$ actually vanishes. For these lattices, these pairing terms are expected to occur even in the absence of spontaneous symmetry breaking. As a consequence, none of the QSL ground states of these lattices exhibit a Majorana Fermi surface, but a nodal line structure instead [3].

[18] A third type of interaction term involving a Majorana and its three neighboring sites [e. g. , $c_1(R)c_2(R)c_3(R)c_4(R - a_3)$] turns out to be forbidden by time-reversal symmetry.

[19] As explained in detail in the Supplemental Material [20], one has to ensure by a combination of real-space and gauge transformations that one remains in the same (free-flux) gauge sector (of the ground state) when implementing the symmetries.

[20] See Supplemental Material at http://link.aps.org/supplemental/10.1103/PhysRevLett.115.177205, which includes Ref. [21], for a visualization of the lattice distortion in the E phase, which is determined entirely by the remaining symmetries of the lattice.

[21] M. I. Aroyo, J. M. Perez-Mato, C. Capillas, E. Kroumova, S. Ivantchev, G. Madariaga, A. Kirov, and H. Wondratschek, Bilbao Crystallographic Server: I. Databases and crystallographic computing programs, Z. Krist. **221**, 15 (2006).

[22] A. J. Leggett, A theoretical description of the new phases of liquid ^{3}He, Rev. Mod. Phys. **47**, 331 (1975).

[23] For our calculation we assume that T_c remains well below the gap for flux-loop excitations, which we do not include in our treatment. The numerical value of the flux gap is $\approx 0.18J$ for the hyperoctagon model at hand. Note that some of the T_c values in the middle panel of Fig. 3 overshoot this value due to the relatively large value of U chosen for this illustration.

[24] T. Senthil and M. P. A. Fisher, $\mathbb{Z}_2$ gauge theory of electron fractionalization in strongly correlated systems, Phys. Rev. B **62**, 7850 (2000).

[25] J. Nasu, M. Udagawa, and Y. Motome, Vaporization of Kitaev Spin Liquids, Phys. Rev. Lett. **113**, 197205 (2014).

[26] I. Kimchi, J. G. Analytis, and A. Vishwanath, Three-dimensional quantum spin liquids in models of harmonic-honeycomb iridates and phase diagram in an infinite-D approximation, Phys. Rev. B **90**, 205126 (2014).